Manipulation of Majorana Modes in a Double Quantum Dot

Jesus D. Cifuentes[1] and Luis G. G. V. Dias da Silva[1]

[1] *Instituto de Física, Universidade de São Paulo, C.P. 66318, 05315–970 São Paulo, SP, Brazil*

(Dated: January 11, 2019)

Majorana fermions appearing at the edges of topological superconducting wires are a promising platform for fault-tolerant quantum computation. Novel proposals use Majorana modes tunneling inside quantum dots (QDs) to implement quantum architectures, because todays precise experimental control over the QD parameters offers the unique possibility of manipulating the Majorana modes inside multi-dot systems. The simplest case where Majorana manipulation is possible is in a double quantum dot (DQD). So far, no complete analysis of this basic structure has been done. This project fills this gap by realizing an exact quantum transport study of the effects of coupling a Majorana mode with a DQD. By tuning the model parameters we show that it is possible to control the localization of the Majorana signature in the DQD.

I. INTRODUCTION

In the last few decades the interest in the so called Majorana fermions has been increasing. The particle proposed by the physicist Ettore Majorana as the real field solution of the Dirac equation describes a fermion which is its own antiparticle, hence it has no charge nor mass. To the date no fundamental particle with these characteristics has been found. However, theoretical research predicts that Majorana Fermions emerge as quasi-particles at the boundary of certain topological superconductors. Kitaev [1] Recently, the new technological innovations allowed the observation of Majorana signatures in different topological materials.[2–5]

Despite the positive experimental results, their is still certain skepticism about the existence of Majorana Fermions. One of the reasons is that some properties of Majorana quasiparticles like the expected non-abelian statistics have not been measure. This property is of especial interest due to its promising applications in topological quantum computing. The braiding protocol based on Majorana's non-abelian statistics is the key to fault-tolerant quantum computation.[6,7]

A promising method to detect Majorana modes consists in attaching a quantum dot (QD) to the edges of a Majorana chain in the topological phase and executing transport measurements through the QD.[8] The Majorana mode at the end of the chain then leaks inside the QD[9] which produces a zero-bias conductance peak of half a quanta $\frac{e^2}{2h}$ through the dot. This is a Majorana signature which produces half of the expected peak by a regular fermion. Recently, experiments including hybrid Majorana-QD systems have been performed.[10] In addition, the similarity of this phenomenon with the Kondo effect,[11,12] where the zero-bias conductance peak takes $\frac{e^2}{h}$, motivated the study of combined Kondo-Majorana physics in this system.[13,14] This project revealed the existance of a region of parameters where both, Kondo and Majorana physics, coexist.

This idea has turned on new lights into the design of quantum architectures,[15,16] because todays precise experimental control over the parameters of QDs - energy levels, tunneling couplings, etc. - offers the unique possibility of manipulating the Majorana modes inside multi-dot systems. The simplest case where Majorana manipulation is possible is in a double quantum dot. So far, no complete analysis of this simple case has been done. The goal of this project is to fill this gap by realizing a full quantum transport study of the effects of coupling a Majorana mode with a double quantum dot. By tuning the QD gate voltages and the Majorana couplings we will be able to probe the mobility of the Majoranamodes through the dots.

We considered both interacting and non-interacting cases. For interacting systems we used a obtained the exact transport description . On non-interacting models we used a NRG approach. We found that in symmetric couplings In the non-interacting case, we confirmed that shifting the QDs gate voltage induces the Majorana to tunnel only to the other dot. In addition, an indirect coupling of the second dot could cause destructive interference with the Majorana signature. In the interacting case, the NRG simulations confirmed these results and showed that other interacting effects - Kondo effect and RKKY interactions[17–19] - could coexist with the Majorana signatures. On the other hand, when only one QD is coupled to the leads and the other Dot is attached to the QD, the Kondo effect is annihilated due to the destructive interference generated by extra dot.[20] Our study includes how the Majorana mode interacts with these two effects.

II. MODEL AND METHODS

We consider the setup shown in Figure 7 in which a Majorana mode at the edge of Topological Superconductor(TS) is coupled to a double quantum dot (DQD), which is attached to a single metallic lead. The Hamiltonian of this system can be partitioned in four terms: the DQD Hamiltonian H_{DQD} , the Lead Hamiltonian H_{Lead} , the DQD-lead interaction $H_{DQD-Lead}$ and the coupling between the DQD and the Majorana mode H_{M-DQDs} and

$$H = H_{DQD} + H_{Lead} + H_{DQD-Lead} + H_{M-DQD} \quad (1)$$

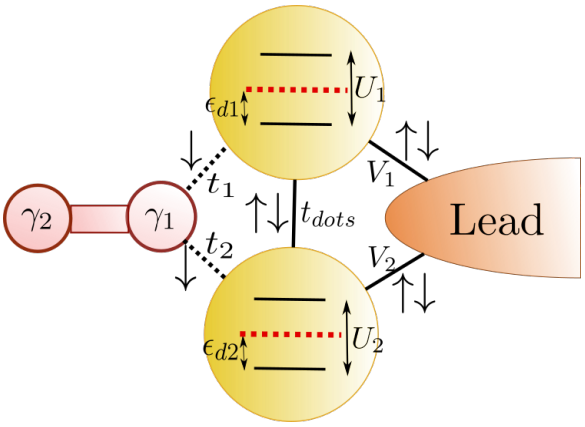

FIG. 1: DQD-Majorana set-up. Solid lines: standard coupling. Dashed lines: Majorana spin-↓ effective couplings (6). The atomic energy levels appear inside each QD. Red dashed horizontal lines represent the Fermi level.

The interacting Anderson Model describes the DQD-lead system

$$H_{DQD} = \sum_{i\in\{1,2\}} \sum_{\sigma\in\{\downarrow,\uparrow\}} \left(\epsilon_{di} + \frac{U_i}{2}\right) \hat{n}_{i\sigma} + \frac{U_i}{2}(\sum_{\sigma} \hat{n}_{i\sigma} - 1)^2 + \sum_{\sigma\in\{\uparrow,\downarrow\}} t_{dots}(d^\dagger_{1\sigma} d_{2\sigma} + d^\dagger_{2\sigma} d_{1\sigma}), \tag{2}$$

and

$$H_{Lead} = \sum_{\mathbf{k}\sigma} \epsilon_{\mathbf{k}} c^\dagger_{\mathbf{k}\sigma} c_{\mathbf{k}\sigma} \tag{3}$$

$$H_{DQD-Lead} = \sum_{\mathbf{k}\sigma} \sum_{i\in\{1,2\}} V_{i\mathbf{k}} c^\dagger_{\mathbf{k}\sigma} d_{i\sigma} + V^*_{i\mathbf{k}} d^\dagger_{i\sigma} c_{\mathbf{k}\sigma}, \tag{4}$$

where ϵ_{di} is the energy level of dot i, U_i is the Coulomb repulsion and t_{dots} is the coupling parameter between both QDs. The operator $d^\dagger_{i\sigma}$ creates a particle in dot i with spin σ and $\hat{n}_{i\sigma} := d^\dagger_{i\sigma} d_{i\sigma}$ is the particle number operator of state i. $c^\dagger_{\mathbf{k}\sigma}$ is the creation operator a particle with momentum $\mathbf{k}$ and spin σ in the lead. $\epsilon_{\mathbf{k}l}$ is the corresponding energy and $V_i(\mathbf{k})$ describes the tunneling coupling between the lead and dot i .

The Majorana modes are modeled as a superposition of the creation and annihilation operators of a spin ↓ particle $f_\downarrow$

$$\gamma_1 := \frac{1}{\sqrt{2}}\left(f^\dagger_\downarrow + f_\downarrow\right), \gamma_2 := \frac{i}{\sqrt{2}}\left(f^\dagger_\downarrow - f_\downarrow\right). \tag{5}$$

This makes possible to define an effective coupling between the Majorana Mode and the DQD by attaching γ_1 with the spin-↓ channel in the QDs

$$H_{M-DQD} = \sum_{i=1}^{2} t_i \left(d^\dagger_{i\downarrow}\gamma_1 + \gamma_1 d_{i\downarrow}\right) + \epsilon_M \gamma_1 \gamma_2. \tag{6}$$

where t_i is the coupling parameter between the Majorana mode and QD i. ϵ_m is the coupling energy between both Majorana modes.

A. Methods

B. Non-interacting case

To study the non-interacting case ($U = 0$), we use Zubarev's ballistic transport approach[21] to compute the Green functions associated to both quantum dot operators $(G_{d_1 d_1^\dagger}(\omega), G_{d_2 d_2^\dagger}(\omega))$. The detailed procedure is included in Appendix A. The transport equations define a linear system where the Hamiltonian parameters $(t_1, t_2, \epsilon_1 \ldots)$ and the energy ω are taken as fix variables. The flow graph in FIG.2 depicts the linear map associated to the transport in an hybrid Majorana-DQD system (A6) . The energies of each operator are located at the center of the vertexes while the vertex couplings represent the off-diagonal terms. The Majorana mode connects two regions of the graph, both of them representing a DQD. The upper DQD is conformed by annihilation operators while the lower one is formed by creation operators. The couplings in the lower part are the upper parameters multiplied by -1.

To simplify the solution of this system we used a graph linear algorithm that speeds-up the process of Gauss-Jordan elimination.[22] Starting with the flow graph at FIG.2 (a), the algorithm successively "pops" the vertexes till only one vertex remains in the graph. Popping a vertex must be understood as the Gaussian elimination of the line and the column in the transport matrix containing that vertex (Appendix A). This modifies the energies of the vertexes and the coupling parameters. Changing the order of elimination of the vertexes could lead to different equivalent representations of the final polynomial. Finding a suitable elimination order could significantly reduce the complexity of the solution.[22]

This graph-linear solver algorithm turns out to be particularly good for Majorana systems since the Majorana fermion is a natural cutting point that divides the graph in two sections. This allows us to exploit the graph structure to simplify the solution of the system by selecting a suitable order of vertex-elimination . Fig.2 depicts this process. In the first step (a) to (b), we pop consecutively the vertexes $c_{k,\downarrow}, c^\dagger_{k,\downarrow}, d_{2,\downarrow}, d^\dagger_{2,\downarrow}$. The new parameters $\epsilon^{\pm}_{DQD}$, M_2 and $T_\pm$ (See Appendix A) are functions of $\epsilon_1, \epsilon_2, t_1, t_2$, etc . These functions gather the transport information through the popped vertexes . The next step is to pop vertexes $d^\dagger_{1,\downarrow}$ and $f_\downarrow$, which condensed the transport information of the whole system into the remaining

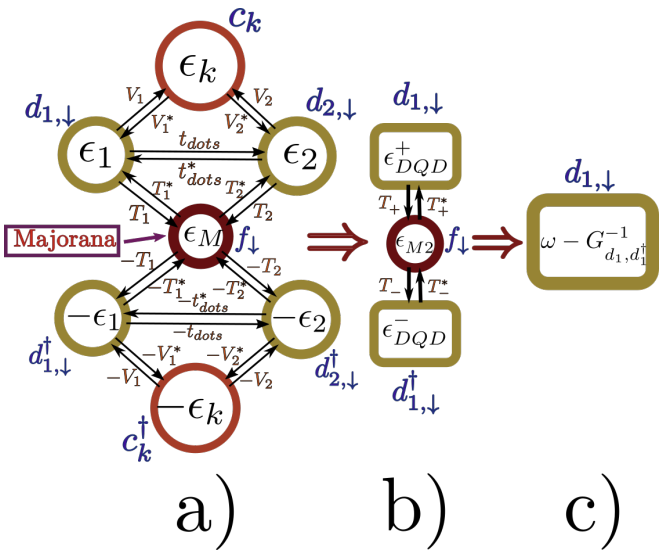

FIG. 2: Transport flow in a DQD Majorana system.

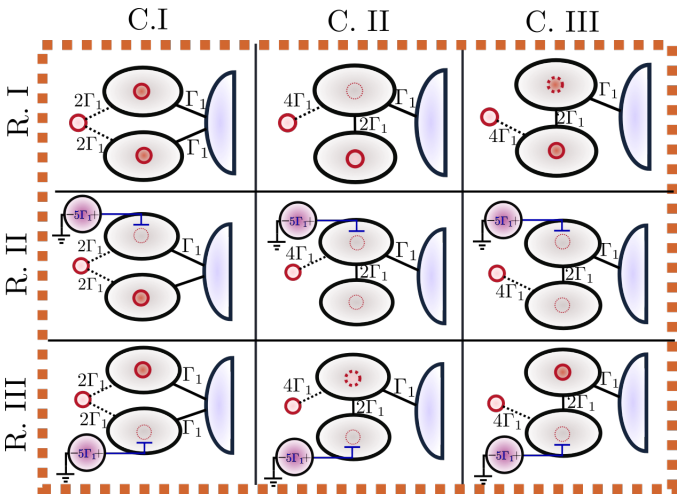

FIG. 3: Manipulation of majorana signatures according to the different connections

vertex $d_{1,\downarrow}$. As shown in Appendix A the energy of vertex $d_{1,\downarrow}$ is $\omega - G_{d_1\downarrow d_1^\dagger\downarrow}(\omega)$, hence giving a very compact expression for the Green function

$$G_{d_{1\downarrow},d_{1\downarrow}^\dagger}(\omega) = \frac{1}{\omega - \epsilon_{DQD}^{+} - \frac{\|T_+\|^2}{\omega-\epsilon_{M2}-\frac{\|T_-\|^2}{\epsilon_{DQD}^{-}}}}. \quad (7)$$

The final result will depend on the broadening parameter of QD i with the lead (Γ_i). This broadening satisfies the equation

$$-i\Gamma_i = \lim_{s\to 0}\sum_{\boldsymbol{k}} \frac{V_i^* V_i}{\omega + is - \epsilon_{\boldsymbol{k}}}. \quad (8)$$

By convention we will take Γ_1 as the energy unit for the rest of the project. Finally we compute the DOS

$$\rho_{1\sigma}(\omega) = -\frac{1}{\pi}\mathrm{Im}\left[G_{d_{1\sigma},d_{1\sigma}^\dagger}(\omega))\right]. \quad (9)$$

Similar results can be obtain for the DOS of the second $\rho_{2\sigma}$. Comparing these results for both dots at the Fermi energy we will be able to determine which dot exhibits a Majorana signature.

C. Interacting case (NRG)

For the interacting case, we used the Numerical Renormalization Group (NRG) approach[12,23,24]. The algorithm assumes a coulomb repulsion of $U = 17.3\Gamma_1$ at both dots and a cut-off energy $D = 2U = 34.6\Gamma_1$. The spacing between the nearest energy levels is assumed to be higher than D, hence only one level is relevant in dynamics of the system. Particle-Hole-Symmetry at each dot is obtained when $\epsilon_i = \frac{U}{2}$. At this point, there is an odd number of electrons at each dot. Hence, at sufficiently low temperature the system will exhibit the characteristic Kondo peak Wilson[12]. Observing how the Kondo-effect interacts with the Majorana signature in the double quantum dot is also an insight of this project.

To improve the efficiency of the code we took advantage of the preserved symmetries: The spin-↑ particle number $\hat{N}_\uparrow$ and the spin-↓ parity $\hat{P}_\downarrow = \pm$ (+ even, − odd). The spin-↓ particle number is not preserved due to the majorana coupling (6) . The initial Hamiltonian is organized in blocks according to these symmetries. This block structure is preserved during the entire iteration process[24]. To compute the spectral functions we use the density matrix renormalization group (DM-NRG) approach.[25]

III. RESULTS

A. Majorana manipulation in non-interacting quantum dots

In non-interacting dots ($U = 0$), the density of states at each dot can be obtained from equation (9) by replacing the green function at (7). The manipulation of the Majorana mode is achieved by tuning the model parameters $(t_1, t_2, \epsilon_1, \epsilon_2, t_dots)$. Fig.3 shows 9 possible processes. The first column shows a symmetric coupling of both QDs with the lead and the Majorana mode. In columns two and three the second dot is attached inderectly to the lead through the first dot. The majorana mode can be either attached to the first dot (column 2) or to the second dot (column 3). In the first row we assume that

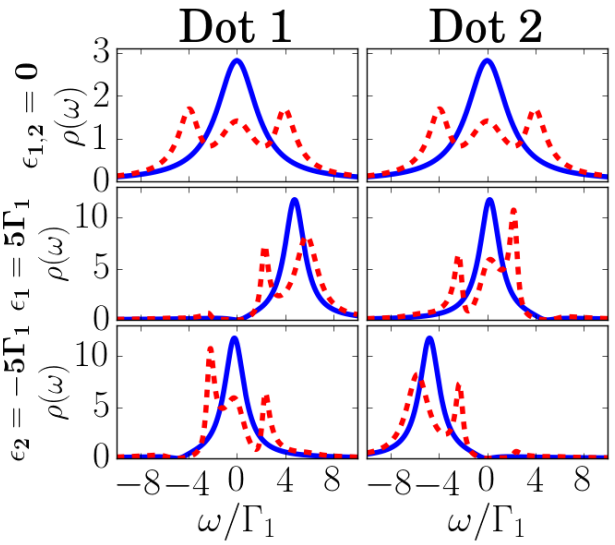

FIG. 4: Density of states in the symmetric coupling arrangement (Fig.3 first column). Solid lines: Spin-↑ DOS. Dashed lines: Spin-↓ DOS.

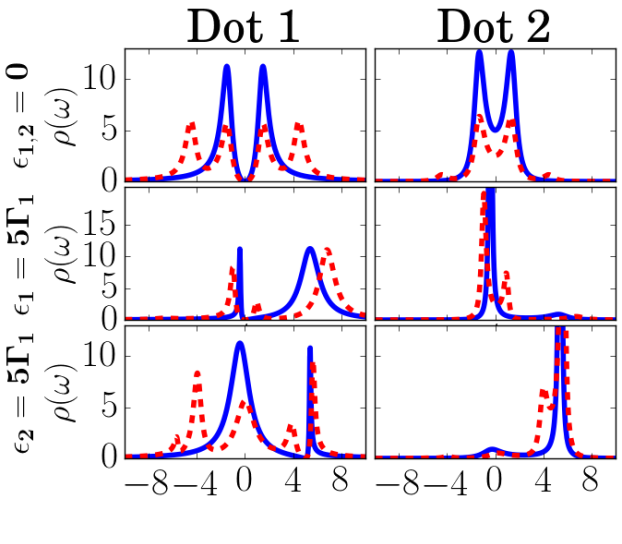

FIG. 5: Density of states in both dots of the case where the only the first QD is attached to both Majorana and Lead (Fig.3 second column) . Solid lines: Spin-↑ DOS. Dashed lines: Spin-↓ DOS.

the gate voltage through both dots is 0 ($\epsilon_1 = \epsilon_2 = 0$), hence the density of states is particle hole symmetric ($\rho(\omega) = \rho(-\omega)$). The majorana signature can be manipulated by increasing the gate voltage at QD1 (second row) or QD2(third row).

The density of states for the set-ups in column 1 (FIG.3) is shown in Figure 4. Since the model is non-interacting, spin-↑ and spin-↓ models are independent. The spin-↓ DOS (dashed line) shows the effects caused by the majorana mode in comparison with the spin-↑ results (solid line). In the particle hole symmetric case the DOS is equal in both dots. Note that that the spin-↓ DOS is the half of the spin-*DOS* at the fermi energy $\rho_\downarrow(0) = \rho_\uparrow(0)$. This is a Majorana signature similar to the one observed in the single dot case[8]. Hence, the majorana tunnels inside both dots. When a possitive or negative gate voltage is induced in one of the dots, the Majorana mode is induced to leave that dot. As consequence the majorana signature will only appear in the other dot.

If the second dot is not directly connected to the lead some interesting results appear. In this set-up the induced tunneling between both dots generated a path difference that destroys the central peak (See FIG5 spin-↑ line). If the Majorana mode is connected to the first dot, this interference will destroy the majorana signature in the first dot. Interestingly, it is possible to observe a clear majorana signature in the second dot caracterized by a half central peak in the spin-*dw* DOS. While turning on the first dot gate volge seems to destroy this majorana signature, tuning the second dots gate voltage returns the majorana signature to the first dot.

On the other hand, if the Majorana mode is attached to the second dot in the previous arrangement, then both dots will exhibit a majorana signature. However, the signature in dot 1 is different from the others. The spin-↓ DOS reveals the emergence of a zero mode with height close to 5.2 (such that $\pi\Gamma_1\rho_\downarrow(0) = 0.5$). However the spin-↑ DOS remains equal to 0. This new type of majorana signature is the result of an indirect connection between QD1 and the majorana mode attached t the second dot. As in the previous case, turning on the gate voltage in dot 1 destroys the majorana signature in both dots. However, if the gate voltage in dot 2 is turned on, the Majorana mode will leave QD2 but the indirect majorana signature will prevail in QD1.

To sum up we were able to distinguish two types of majorana signatures:

- **Type I:** The spin-↓ DOS is the half of the spin-↑ DOS at the Fermi energy ($\rho_\downarrow(0) = \rho_\uparrow(0)$).

- **Type II:** The spin-↓ Fermi energy is equal about 5.2. This is the value such that $\pi\Gamma_1\rho_\downarrow(0) = 0.5$, characteristic of a decay of half a quanta in the conductivity.

The state of these signatures for each of these stated is depicted in FIG.3. A solid filled red circle inside the dot represents the appearance of a Type I Majorana signature, on the othere hand a dashed filled red circle represents the presence a Type II Majorana signature. The obscure dashed circle represents a vanishing majorana signature due to an applied gate voltage or by quantum interference.

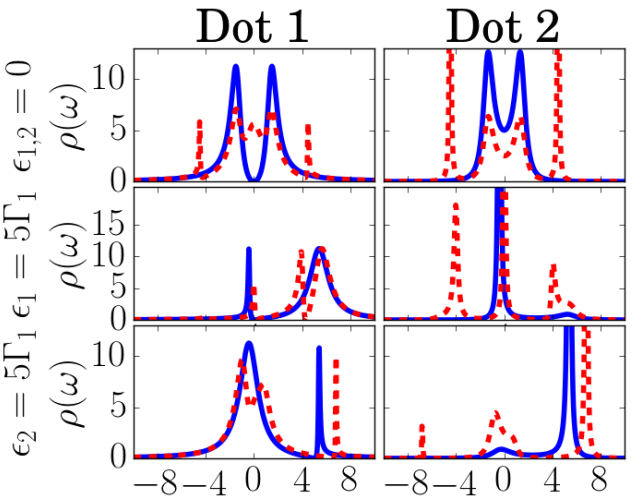

FIG. 6: Density of states of both dots in the case where only de first QD is attached to the lead and the Majorana mode is attached to the second QD. (Fig.3 third column) . Solid lines: Spin-↑ DOS. Dashed lines: Spin-↓ DOS.

B. Majorana manipulation in interacting dots

We consider a Coulomb repulsion energy of $U = 17\Gamma_1$ in both dots. The factor $\frac{U_i}{2}(\sum_\sigma \hat{n}_{i\sigma} - 1)^2$ in (2) favors states with an odd number of electrons. In addition, particle-hole equilibrium is now achieved when $\left(\epsilon_{di} + \frac{U_i}{2}\right)\hat{n}_{i\sigma}$. Any induced gate voltage must be considered as a shifting from this equilibrium point. In the case of symmetric coupling FIG7 shows the DOS in both QDs. The two peaks appearing at $8.6\Gamma_1 = \frac{U_i}{2}$ represent the two energy levels. The central spin-↑ peak is produced by the Kondo effect,[11,12] while the two satellite peaks observed in the inset observed are the result of the RKKY anti-ferromagnetic interaction between bott dots.[17–19] The spin-↓ DOS at the fermi energy is exactly the half of the spin-↑ DOS as expected from a Type I majorana signature. Note, that in this case the majorana signature coexists with the Kondo effect in the DQD as already predicted by Ruiz-Tijerina *et al.* for a single dot.[14]

IV. CONCLUDING REMARKS

Conclusion goes here.

ACKNOWLEDGMENTS

The authors thank Edson Vernek for enlightening discussions. L.G.G.V.D.S. acknowledges financial support by CNPq (grants No. 307107/2013-2 and 449148/2014-9), and FAPESP (grant No. 2016/18495-4).

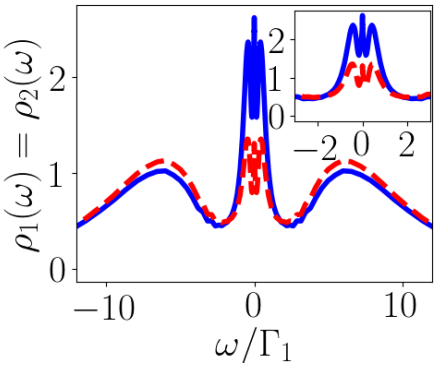

FIG. 7: Density of states of both dots in the symmetric coupling case between the Majorana and the interacting DQD. Solid lines: Spin-↑ DOS. Dashed lines: Spin-↓ DOS.

[1] A. Y. Kitaev, Physics-Uspekhi **44**, 131 (2001).
[2] V. Mourik, K. Zuo, S. M. Frolov, S. R. Plissard, E. P. a. M. Bakkers, and L. P. Kouwenhoven, Science **336**, 1003 (2012).
[3] A. Das, Y. Ronen, Y. Most, Y. Oreg, M. Heiblum, and H. Shtrikman, Nature Physics **8**, 887 (2012).
[4] M. T. Deng, C. L. Yu, G. Y. Huang, M. Larsson, P. Caroff, and H. Q. Xu, Nano Letters **12**, 6414 (2012).
[5] H. Zhang, C.-X. Liu, S. Gazibegovic, D. Xu, J. A. Logan, G. Wang, N. van Loo, J. D. S. Bommer, M. W. A. de Moor, D. Car, R. L. M. Op het Veld, P. J. van Veldhoven, S. Koelling, M. A. Verheijen, M. Pendharkar, D. J. Pennachio, B. Shojaei, J. S. Lee, C. J. Palmstrm, E. P. A. M. Bakkers, S. D. Sarma, and L. P. Kouwenhoven, Nature **556**, 74 (2018).
[6] A. Y. Kitaev, Annals of Physics **303**, 2 (2003), arXiv: quant-ph/9707021.
[7] S. D. Sarma, M. Freedman, and C. Nayak, npj Quantum Information **1**, 15001 (2015).
[8] D. E. Liu and H. U. Baranger, Physical Review B **84** (2011), 10.1103/PhysRevB.84.201308, arXiv: 1107.4338.
[9] E. Vernek, P. H. Penteado, A. C. Seridonio, and J. C. Egues, Physical Review B **89**, 165314 (2014).
[10] M. T. Deng, S. Vaitiekenas, E. B. Hansen, J. Danon, M. Leijnse, K. Flensberg, J. Nygard, P. Krogstrup, and C. M. Marcus, Science **354**, 1557 (2016).
[11] A. C. Hewson, *The Kondo Problem to Heavy Fermions* (Cambridge University Press, 1997) google-Books-ID: fPzgHneNFDAC.
[12] K. G. Wilson, Reviews of Modern Physics **47**, 773 (1975).

[13] M. Lee, J. S. Lim, and R. Lopez, Physical Review B **87**, 241402 (2013).
[14] D. A. Ruiz-Tijerina, E. Vernek, L. G. G. V. Dias da Silva, and J. C. Egues, Physical Review B **91**, 115435 (2015).
[15] M. Barkeshli and J. D. Sau, arXiv:1509.07135 [cond-mat, physics:quant-ph] (2015), arXiv: 1509.07135.
[16] T. Karzig, C. Knapp, R. M. Lutchyn, P. Bonderson, M. B. Hastings, C. Nayak, J. Alicea, K. Flensberg, S. Plugge, Y. Oreg, C. M. Marcus, and M. H. Freedman, Physical Review B **95**, 235305 (2017).
[17] M. A. Ruderman and C. Kittel, Physical Review **96**, 99 (1954).
[18] T. Kasuya, Progress of Theoretical Physics **16**, 45 (1956).
[19] K. Yosida, Physical Review **106**, 893 (1957).
[20] L. G. G. V. Dias da Silva, N. Sandler, K. Ingersent, and S. E. Ulloa, Physica E: Low-dimensional Systems and Nanostructures **40**, 1002 (2008).
[21] D. N. Zubarev, Soviet Physics Uspekhi **3**, 320 (1960).
[22] D. A. Spielman, *Algorithms, Graph Theory, and Linear Equations in Laplacian Matrices*, Proceedings of the International Congress of Mathematicians (2010).
[23] M. Sindel, *Numerical Renormalization Group studies of Quantum Impurity Models in the Strong Coupling Limit*, Text.PhDThesis, Ludwig-Maximilians-Universitt Mnchen (2005).
[24] R. Bulla, T. A. Costi, and T. Pruschke, Reviews of Modern Physics **80**, 395 (2008).
[25] W. Hofstetter, Physical Review Letters **85**, 1508 (2000).

Appendix A: Computation of the Green Function

In Zubarev's fermionic ballistic transport approach[21] the green functions associated to two operators $A(t)$, $B(t)$ is defined as that Fourier transform of the time-ordered anti-commutator of A and B

$$G_{A,B}(\omega) = \mathcal{F}\left\{\mathcal{T}\left[\{A(t), B(t')\}\right]\right\}(\omega)\,. \tag{A1}$$

The Fourier transform of Schrodinger evolution determines the transport equations

$$\omega G_{A,B}(\omega) = \delta_{A^\dagger,B} + G_{[A,H],B}(\omega). \tag{A2}$$

We can apply this to Hamiltonian (1) by replacing A and B by the creation and annihilation operators. To simplify the complexity of the system we fix $B = d^\dagger_{1\downarrow}$. In addition note that the transport equations for $f_\downarrow$ and $f^\dagger_\downarrow$ are

$$(\omega - \epsilon_M)\, G_{f_\downarrow, d^\dagger_{1\downarrow}}(\omega) = \frac{t}{\sqrt{2}}\left(G_{d_{1\downarrow}, d^\dagger_{1\downarrow}}(\omega) - G_{d^\dagger_{1\downarrow}, d^\dagger_{1\downarrow}}(\omega)\right) \tag{A3}$$

$$(\omega + \epsilon_M)\, G_{f^\dagger_\downarrow, d^\dagger_{1\downarrow}}(\omega) = \frac{t}{\sqrt{2}}\left(G_{d_{1\downarrow}, d^\dagger_{1\downarrow}}(\omega) - G_{d^\dagger_{1\downarrow}, d^\dagger_{1\downarrow}}(\omega)\right), \tag{A4}$$

which allows us to take $G_{f^\dagger_\downarrow, d^\dagger_{1\downarrow}}(\omega) = \frac{\omega+\epsilon}{\omega-\epsilon} G_{f^\dagger_\downarrow, d^\dagger_{1\downarrow}}(\omega)$. Therefore, we can eliminate $G_{f^\dagger_\downarrow, d^\dagger_{1\downarrow}}(\omega)$ from the equations even before we start Gauss-Jordan process.

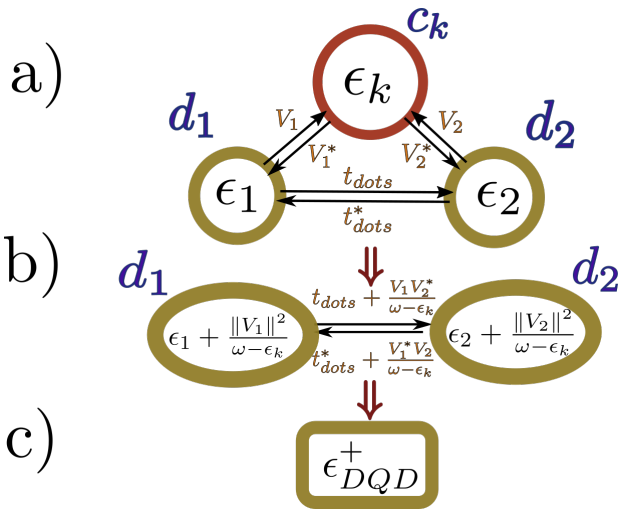

FIG. 8

Writing the other equations we obtain the linear system

$$\mathcal{T}\vec{G}_{d^\dagger_1} = \hat{e_1} \tag{A5}$$

where $\mathcal{T}$ is the transport matrix

$$\begin{bmatrix}
\omega-\epsilon_1 & -V_1^* & -t_{dots} & \frac{-t_1}{\sqrt{2}} & 0 & 0 & 0 \\
-V_1 & \omega-\epsilon_k & -V_2 & 0 & 0 & 0 & 0 \\
-t^*_{dots} & -V_2^* & \omega-\epsilon_2 & \frac{-t_2}{\sqrt{2}} & 0 & 0 & 0 \\
\frac{-\sqrt{2}t_1^*}{\omega+\epsilon_M} & 0 & \frac{-\sqrt{2}t_2^*}{\omega+\epsilon_M} & \omega-\epsilon_M & \frac{\sqrt{2}t_2^*}{\omega+\epsilon_M} & 0 & \frac{\sqrt{2}t_1^*}{\omega+\epsilon_M} \\
0 & 0 & 0 & \frac{t_2}{\sqrt{2}} & \omega+\epsilon_2 & V_2^* & t^*_{dots} \\
0 & 0 & 0 & 0 & V_2 & \omega+\epsilon_k & V_1 \\
0 & 0 & 0 & \frac{t_1}{\sqrt{2}} & t_{dots} & V_1^* & \omega+\epsilon_1
\end{bmatrix}, \tag{A6}$$

$\vec{G}_{d^\dagger_1}$ is the column vector

$$[G_{d_{1\downarrow}, d^\dagger_{1\downarrow}}(\omega), G_{c_{k\downarrow}, d^\dagger_{1\downarrow}}(\omega), G_{d_{2\downarrow}, d^\dagger_{1\downarrow}}(\omega), G_{f_\downarrow, d^\dagger_{1\downarrow}}(\omega), G_{d^\dagger_{2\downarrow}, d^\dagger_{1\downarrow}}(\omega), G_{c^\dagger_{k\downarrow}, d^\dagger_{1\downarrow}}(\omega), G_{d^\dagger_{1\downarrow}, d^\dagger_{1\downarrow}}(\omega)]^T$$

and $\hat{e_1}$ is the vector with entries $\hat{e}_{1_n} = \delta_{1n}$.

The graph associated to this matrix is the one in FIG.2. The energies inside each vertex are given by subtracting the corresponding diagonal term from ω . The couplings are just the negative of the off-diagonal terms.

1. The double quantum dot

To explain the process of Gaussian elimination we will obtain the green function for the case without Majorana fermion ($t_1 = t_2 = 0$). The transport matrix for this system is

$$\begin{bmatrix}
\omega-\epsilon_1 & -V_1 & -t_{dots} \\
-V_1^* & \omega-\epsilon_k & -V_2 \\
-t^*_{dots} & -V_2^* & \omega-\epsilon_2
\end{bmatrix}. \tag{A7}$$

The graph associated to this matrix can be observed in FIG8.a). To eliminate the vertex c_k we just need to subtract from (A7) the rank-1 matrix that cancels the row and the column corresponding to c_k. This matrix is

$$\begin{bmatrix} \frac{V_1^* V_1}{\omega-\epsilon_k} & -V_1^* & \frac{V_2 V_1^*}{\omega-\epsilon_k} \\ -V_1 & \omega-\epsilon_k & -V_2 \\ \frac{V_2^* V_1}{\omega-\epsilon_k} & -V_2^* & \frac{V_2^* V_2}{\omega-\epsilon_k} \end{bmatrix}. \tag{A8}$$

The result of (A7) - (A8) is

$$\begin{bmatrix} \omega-\epsilon_1-\frac{V_1^* V_1}{\omega-\epsilon_k} & 0 & -t_{dots}-\frac{V_2 V_1^*}{\omega-\epsilon_k} \\ 0 & 0 & 0 \\ -t_{dots}^*-\frac{V_2^* V_1}{\omega-\epsilon_k} & 0 & \omega-\epsilon_2-\frac{V_2 V_1^*}{\omega-\epsilon_k} \end{bmatrix} \tag{A9}$$

which is depicted by the graphs in FIG.8.b). The next step is to pop-out the vertex d_2 following the same procedure. At the end, the energy inside the vertex d_1 will be

$$\epsilon_{DQD}^{+} = \epsilon_1 + \sum_{\mathbf{k}} \frac{V_1 V_1^*}{\omega-\epsilon_{\mathbf{k}}} + \frac{\left\| t_{dots} + \sum_{\mathbf{k}} \frac{V_1 V_2^*}{\omega-\epsilon_{\mathbf{k}}} \right\|^2}{\omega-\epsilon_2-\sum_{\mathbf{k}} \frac{V_2 V_2^*}{\omega-\epsilon_{\mathbf{k}}}} \tag{A10}$$

and the green function of $G_{d_1 d_1^\dagger}(\omega)$ in a DQD will be given by $\frac{1}{\omega-\epsilon_{DQD}}$ (see FIG.8.c)).

2. Solution of the transport equations

The previous procedure can be generalized into the following algorithm:

1. Computing the transport equations with the second term fixed in the creation operator of the dot.
2. Setting up the graph associated to the transport system.
3. Popping out the vertexes of the graph. Each popping process carries the following steps.
   (a) Computing the extra-terms in the energies and couplings based on the walks passing through the popped vertex.
   (b) Eliminating this vertex from the graph.
   (c) Iterating till there is only one vertex.
4. The energy in the remaining vertex d is $\epsilon_d = \frac{1}{\omega-G_{d,d^\dagger}(\omega)}$.

Following these steps it is possible to solve the general case. We start with the graph in FIG.2 and we pop out the vertexes $c_k, c_k^\dagger, d_{2,\downarrow}$ and $d_{2,\downarrow}^\dagger$ in that order. The energies associated to $d_{1,\downarrow}$ and $d_{1,\downarrow}^\dagger$ will be similar to (A10) giving

$$\epsilon_{DQD}^{\pm} = \pm\epsilon_1 + \sum_{\mathbf{k}} \frac{V_1 V_1^*}{\omega-\epsilon_{\mathbf{k}}} + \frac{\left\| \pm t_{dots} + \sum_{\mathbf{k}} \frac{V_1 V_2^*}{\omega-\epsilon_{\mathbf{k}}} \right\|^2}{\omega \pm \epsilon_2 - \sum_{\mathbf{k}} \frac{V_2 V_2^*}{\omega-\epsilon_{\mathbf{k}}}}. \tag{A11}$$

There is also a correction in the couplings between the Majorana mode and $d_{1,\downarrow}$, $d_{1,\downarrow}^\dagger$ given by

$$T_{\pm} = \pm t_1 \pm t_2 \frac{\left(\pm t_{dots} + \sum_{\mathbf{k}} \frac{V_1 V_2^*}{\omega-\epsilon_{\mathbf{k}}} \right)}{\omega \pm \epsilon_2 \pm \sum_{\mathbf{k}} \frac{V_2 V_2^*}{\omega-\epsilon_{\mathbf{k}}}}. \tag{A12}$$

Finally since the Majorana is in contact with dot 2, there is an extra-term appearing in the Majorana energy given by

$$\epsilon_{M2} = \omega - \epsilon_M - \frac{\frac{\omega}{\omega+\epsilon_M} \|t_2\|^2}{\omega-\epsilon_2-\sum_{\mathbf{k}} \frac{V_2 V_2^*}{\omega-\epsilon_{\mathbf{k}}}} - \frac{\frac{\omega}{\omega+\epsilon_M} \|t_2\|^2}{\omega+\epsilon_2-\sum_{\mathbf{k}} \frac{V_2 V_2^*}{\omega+\epsilon_{\mathbf{k}}}}. \tag{A13}$$

With all the terms of the graph in FIG.2.b) computed, it only remains to pop out vertexes $d_1^\dagger$ and $f_\downarrow$ in that order to obtain the green function in equation (7).